Multivariate High-Dimensional Cortical Folding Analysis, Combining Complexity and Shape, in Neonates with Congenital Heart Disease

Suyash P. Awate[1], Paul Yushkevich[1], Zhuang Song[1], Daniel Licht[2], and James C. Gee[1]

[1] Penn Image Computing and Science Lab (PICSL), University of Pennsylvania
awate@mail.med.upenn.edu
[2] Children's Hospital of Philadelphia, USA*

Abstract. The paper presents a novel statistical framework for cortical folding pattern analysis that relies on a rich *multivariate descriptor* of folding patterns in a region of interest (ROI). The ROI-based approach avoids problems faced by spatial-normalization-based approaches stemming from the severe deficiency of homologous features between typical human cerebral cortices. Unlike typical ROI-based methods that summarize folding complexity or shape by a single number, the proposed descriptor unifies *complexity* and *shape* of the surface in a *high-dimensional* space. In this way, the proposed framework couples the reliability of ROI-based analysis with the richness of the novel cortical folding pattern descriptor. Furthermore, the descriptor can easily incorporate additional variables, e.g. cortical thickness. The paper proposes a novel application of a nonparametric permutation-based approach for statistical hypothesis testing for any multivariate high-dimensional descriptor. While the proposed framework has a rigorous theoretical underpinning, it is straightforward to implement. The framework is validated via simulated and clinical data. The paper is the first to quantitatively evaluate cortical folding in neonates with complex congenital heart disease.

1 Introduction

Cerebral cortical folding forms an underpinning for the cognitive skills and behavioral traits in humans. It is one of the major maturational processes of the human brain that occurs rapidly throughout fetal and early postnatal life. For the last few decades, the use of magnetic resonance (MR) imaging has enabled in vivo studies of human cortical folding patterns. Several studies relate abnormalities in the *complexity* of folding patterns to neurodevelopmental disorders [1,2].

* The authors gratefully acknowledge the support of this work via NIH grants HD042974, HD046159, NS045839, EB06266, DA14129, DA22807, UL1RR024234, K23 NS052380, NS061111, K25 AG027785, the Dana Foundation, the June and Steve Wolfson Family Foundation, and the Institute for Translational Medicine and Therapeutics' (ITMAT) Transdisciplinary Awards Program in Translational Medicine and Therapeutics at the University of Pennsylvania.

J.L. Prince, D.L. Pham, and K.J. Myers (Eds.): IPMI 2009, LNCS 5636, pp. 552–563, 2009.

While several pioneering studies track the progress of normal cortical folding in foetuses and neonates [3,4,5], others study cortical-folding abnormalities in neonates [6,7] based on subjective clinical protocols.

This paper studies cortical folding in the operculum in neonates with complex congenital heart disease (CHD). The operculum includes language areas and the sensory motor cortex for the mouth, tongue, and throat. There is growing evidence of immature features or frankly delayed maturation of the brains of full-term infants with complex CHD [8,9]. This immaturity likely gives rise to unexpected vulnerability to a white matter injury termed periventricular leukomalacia (PVL), an injury previously seen only in premature infants. Abnormally low fetal blood oxygenation and blood flow and the brain are likely the cause of this maturational delay. While direct evidence is lacking, there are differences in the circulatory patterns in fetuses with different forms of complex CHD. This paper quantitatively evaluates cortical folding in the operculum in two key subtypes of CHD, namely hypoplastic left heart syndrome (HLHS) and transposition of the great arteries (TGA). The paper reports differences in *not* only the complexity of opercular folding patterns, but also their *shape*.

One class of approaches to folding analysis rely on spatial normalization, either volumetric [10,4] or surface-based [2], and subsequently perform statistical hypothesis testing at every voxel or surface-element in the normalized space. Such methods can employ folding descriptors that are curvature-based [10], wavelet-based, etc. In typical cortical studies, however, "dramatic individual differences in the specific pattern of convolutions" [11] make it extremely difficult to find sufficiently-many homologous features [12] that could guarantee a consistent parameterization between cortical surfaces [12,13,11] (see [11] for brain images). Essen and Dierker [11] observe that "no registration that respects the topology of the cortical sheet can successfully match every major and minor fold". While lack of homologies are indeed observed for minor folds, they may occur for some major folds as well [13,11]. The reliability of normalization, because of this natural variability, may directly affect the reliability of findings in the clinical study. Furthermore, because the phenomenon of cortical folding has an inherent large-scale or non-local character, the rationale for point-by-point analysis of folding differences seems unclear.

A second class of approaches propose region-based folding descriptors to quantify folding complexity [14,15,3,5]. Such approaches avoid the problems associated with normalization by reducing spatial sensitivity from a voxel to a region of interest (ROI). ROIs considered in such folding studies can indeed be reliably defined in each individual based on observed homologous features. Such ROIs can be specific structures (e.g. hippocampus), regions around sulci/gyri that are always observable (e.g. operculum), lobes (e.g. frontal), etc.

Most studies in literature based on both aforementioned classes of approaches measure only the complexity of folding patterns, *ignoring* information related to shape, orientation, etc. Although some very recent ROI-based approaches propose descriptors incorporating shape information [16], they fail to integrate all the information on shape and complexity in a single descriptor. Furthermore, typical

ROI-based approaches produce scalar or low-dimensional summary statistics for the entire ROI, risking serious information loss.

This paper makes several contributions. First, the paper presents a novel ROI-based statistical framework for folding pattern analysis relying on a rich multivariate non-local descriptor that captures the spectrum of complexity and shape. Specifically, the descriptor is a joint probability density function (PDF) of two variables, one capturing surface complexity and the other capturing surface shape. Second, the paper proposes a novel application of a nonparametric permutation-based approach for statistical hypothesis testing for the proposed descriptor. In these ways, the proposed framework couples the reliability of ROI-based analysis with the richness of the proposed descriptor. This paper shows that the proposed framework has a rigorous theoretical underpinning and it is straightforward to implement. Third, the proposed hypothesis-testing approach can be easily applied to any multivariate descriptor, e.g. one that augments the proposed cortical-folding descriptor to include cortical-thickness information. Fourth, to the best of our knowledge, this paper is the first to report the affects of HLHS and TGA on opercular folding.

2 Background

2.1 Univariate Low-Dimensional Complexity Descriptors

It is generally important to design folding descriptors that (i) are invariant to *translation* and *rotation* of the cortical surface representation (changes in the location or orientation of the slice planes during MR imaging), and (ii) capture all aspects of folding including *complexity* as well as *shape*.

Some of the earliest folding descriptors were intended to capture *only* the complexity of the cortical surface. Fractal dimension [17,14] captures the increases in surface area over multiscale representations of the surface. Gyrification index [18] is the ratio of the length of a planar curve to the length of the curve's envelope. Convexity ratio [3] is the ratio of the area of the surface to the area of the convex hull/envelope of the surface. Isoperimetric ratio [3] is the ratio of the surface area to the two-third power of the volume enclosed by the surface. Average curvedness (AC) [16] measure the deviation of the surface from a plane. [5] proposes the 2D centroid of the histogram of a curvature.

Some folding descriptors were designed to inform about specific aspects (*not* all) of surface shape. Intrinsic curvature index (ICI) [15] sums up degrees of hemisphericity of all surface patches, but ignores cylindrical or saddle-shaped patches. Mean curvature norm (MCN) [3] sums up degrees of hemisphericity and cylindricity of all surface patches, but ignores saddle-shaped patches. Gaussian curvature norm (GCN) [3] sums up degrees of hemisphericity and saddle-likeness of all surface patches, but ignores cylindrical patches.

While some aforementioned descriptors ignore the *shape* of surface patches, all aforementioned descriptors ignore the *orientation* of surface patches. For instance, they fail to distinguish pimples from dimples or ridges from valleys; these might be compared to cortical gyri and sulci, respectively. Indeed, for

every surface patch, ICI, MCN, GCN, and AC project the space of principal curvatures, having two degrees of freedom, to derive a single scalar descriptor. [5] condense the histogram of a curvature measure to 2 numbers.

2.2 Univariate Low-Dimensional Shape Descriptors

Recent works incorporate information regarding local surface-patch orientation and shape for cortical surface analysis [10,16]. These approaches rely on Koenderink and van Doorn's orthogonal reparameterization of the 2D space of principal curvatures into *shape index* and *curvedness* [19]. Consider a surface $\mathcal{M}$. Let $d\mathcal{M}$ represent the area measure of a small surface patch at point $m \in \mathcal{M}$. At point m, the minimum and maximum principal curvatures of a local patch are denoted by $K_{\min}(m)$ and $K_{\max}(m)$, respectively. Shape index $S : \mathcal{M} \rightarrow [-1, 1]$ for a patch at point m is $S(m) = [2/\pi] \arctan\{[K_{\max}(m)+K_{\min}(m)]/[K_{\max}(m)-K_{\min}(m)]\}$. Shape index values for some standard shapes are: $-1 \equiv$ hemispherical concave, $-0.5 \equiv$ hemicylindrical valley, $0 \equiv$ saddle, $0.5 \equiv$ hemicylindrical ridge, and $1 \equiv$ hemispherical convex. Curvedness $C : \mathcal{M} \rightarrow [0, \infty)$ for a patch at point m is $C(m) = \{0.5[K^2_{\max}(m) + K^2_{\min}(m)]\}^{0.5}$.

Tosun et al. [10] employ the shape index in a voxel-based cortical morphometry scheme. For ROI-based analyses, Awate et al. [16] propose an average shape index, $\mathrm{AS}(\mathcal{M}) = \int_{m \in \mathcal{M}} \mathrm{S(m)}\, d\mathcal{M}$, that averages shape indices of all patches in the ROI. In computer vision, a descriptor corresponding to values of the shape-index histogram at 9 predetermined locations, was proposed recently [20].

All aforementioned approaches in this section ignore cortical complexity in the description of folding patterns. Furthermore, they reduce the information in the shape-index histogram to at most a few numbers (low dimensional).

3 New Multivariate High-Dimensional Folding Descriptor

This section presents a high-dimensional multivariate surface descriptor that captures the spectrum of complexity and shape.

At every point m of a cortical surface $\mathcal{M}$, the principal curvatures *completely* describe the geometry of the local surface patch. The orthogonal parameterization of principal curvatures $< K_{\min}, K_{\max} >$ is, however, unintuitive. This probably motivated reparameterizing $< K_{\min}, K_{\max} >$ into $< C, S >$ [19] to cleanly separate notions of bending and shape, while retaining the orthogonality. Figure 1 shows values of C and S at all points on a typical cortical surface.

We propose the following generative statistical model of cortical surfaces. Let us consider $C : \mathcal{M} \rightarrow [0, \infty]$ and $S : \mathcal{M} \rightarrow [-1, 1]$ as random fields [21]. Let us also consider the joint PDF that captures the dependencies between $C(m)$ and $S(m)$ for a specific class of surfaces. Consider a finite collection $\mathcal{O} = \{d\mathcal{M}^1, \ldots, d\mathcal{M}^T\}$ of T surface patches, located at points $\{m^1, \ldots, m^T\} \in \mathcal{M}$ *uniformly* distributed over the surface $\mathcal{M}$, which form a cover for $\mathcal{M}$. Then, the set $\{(C(m^1), S(m^1)), \ldots, (C(m^T), S(m^T))\}$ is an instantiation of the field of random vectors at locations $\{m^1, \ldots, m^T\}$. We assume that the random

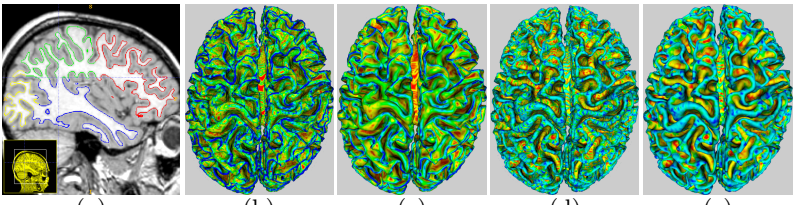

Fig. 1. **(a)** MR image overlapped with the extracted cortical gray-white interface parcellated by lobe. **(b)-(c)** Curvedness $C(m) \geq 0$ values (red→blue ≡ low→high curvature) at each point m on the extracted surface $\mathcal{M}$ and its smoothed version $\mathcal{M}^{\text{smooth}}$, respectively. Note that $\mathcal{M}$ has many more high-curvedness regions than $\mathcal{M}^{\text{smooth}}$. **(d)-(e)** Shape-index $S(m) \in [-1, 1]$ values painted on $\mathcal{M}$ and $\mathcal{M}^{\text{smooth}}$, respectively. Unlike C, S exhibits little change between $\mathcal{M}$ and $\mathcal{M}^{\text{smooth}}$.

field is *stationary* [21], i.e. each observation $(C(m^t), S(m^t))$, is randomly drawn from a single PDF $P_{\mathcal{M}}(C, S)$. The tremendous complexity and inter-individual variability in cortical folding suggests that dependencies between random variables $(C(m^t), S(m^t))$ and $(C(m^s), S(m^s))$ decrease at a fast rate with increasing geodesic distance between the locations m^t and m^s. Thus, we assume that the random field is *mixing* [21].

We propose the joint PDF $P_{\mathcal{M}}(C, S)$ as the multivariate high-dimensional descriptor of cerebral cortical folding patterns for surface $\mathcal{M}$. It is clear that many of the aforementioned univariate descriptors (e.g. ICI, MCN, GCN, AC, AS, histogram centroid, and [20]) are subsumed by the proposed descriptor.

For a given surface $\mathcal{M}$, we propose to estimate $P_{\mathcal{M}}(C, S)$ as follows. Using the sample $\{(C(m^1), S(m^1)), \ldots, (C(m^T), S(m^T))\}$ drawn from a stationary mixing random field, a consistent [22] nonparametric kernel density estimate for the folding descriptor is $P_{\mathcal{M}}(C, S) \approx \frac{1}{T} \sum_{t=1}^{T} G((C(m^t), S(m^t)), \Sigma_t)$, where $G((\mu_1, \mu_s), \Sigma)$ is a 2D Gaussian kernel with mean (μ_1, μ_2) and covariance Σ. Consistency requires an optimal choice of Σ_t, dependent on the sample size T, and we employ a cross-validation-based penalized maximum likelihood scheme to estimate Σ_t [23]; the literature provides a variety of schemes.

It is crucial that the sample $\{m^1, \ldots, m^T\}$ is uniformly distributed over the surface $\mathcal{M}$, eliminating any bias in over/undersampling specific surface features. Nonuniform sampling can undesirably bias $P_{\mathcal{M}}(C, S)$. For instance, adaptively refined meshes will generate more surface patches in areas with larger C and artificially boost the PDF for larger C. Thus, we propose to obtain uniformly-distributed points/patches by representing the surface as a level set of a distance transform on a Cartesian grid [24] sampled at a resolution much higher than the highest C values (see next paragraph). Figure 1 shows a level-set surface colored by the values of C and S, respectively.

This paper represents the level set in a grid of isotropic voxels of size v^3 mm^3 with $v = 0.4$ mm (Figures 1). To reduce effects of noise, level-set fitting incorporates smoothing. Empirically, we find that values $C(m)$ virtually never exceed $c_{\max} = (15v)^{-1}$ mm^{-1} equivalent to a minimum radius of curvature of

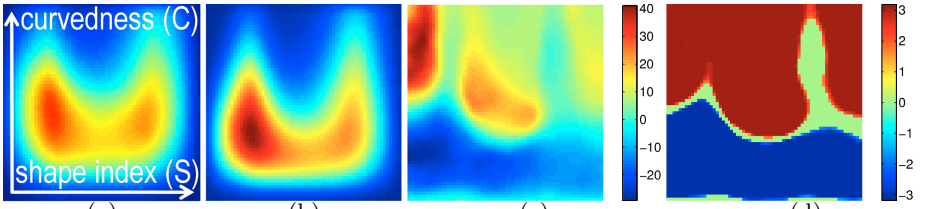

Fig. 2. Validation : a cross sectional study between the group of gray-white interfaces of 20 BrainWeb [26] images and a second group of smoothed versions of the same surfaces. For all plots in this paper, horizontal axis $\equiv S$, vertical axis $\equiv C$, coordinates for the bottom left corner : $(C, S) = (c_{\min}, -1)$; bottom right corner : $(C, S) = (c_{\min}, 1)$; top left corner : $(C, S) = (c_{\max}, -1)$. **(a)-(b)** Mean of the multivariate surface descriptors $P_{\mathcal{M}^n}(C, S)$ for the $n = 1, \ldots, 20$ original and smoothed surfaces, respectively, as proposed in Section 3; red≡high and blue≡low values. **(c)** The t-statistic map for the original and smoothed surfaces; $t > 0 \Rightarrow P_{\text{original}} > P_{\text{smoothed}}$. **(d)** The significant locations ($p < 0.05$) produced via SnPM [25]. For all plots in this paper, p values for significant locations/clusters are indicated by coloring them by the associated z score [21], e.g. $z(p = 0.05) = 1.65$, $z(p = 0.005) = 2.58$.

$15v = 6$ mm. Figures 1 suggests that this degree of smoothing continues to capture essential folding pattern information in typical pediatric cortical surfaces. The lower limit of 6 mm is more conservative than the limit of 3 mm in [5]. Imaging limitations on voxel sizes and signal-to-noise ratios risk less fidelity in capturing sharper surface features.

Figure 2(a) shows a typical $P_{\mathcal{M}}(C, S)$, which is multimodal and far from standard parametric PDFs, thus justifying nonparametric PDF estimation for reliability. In practice, typical ROIs yield sample sizes T in the range of thousands or tens of thousands, producing (i) very small kernel bandwidth estimates such that $P_{\mathcal{M}}(c < 0, s \notin [-1, 1])$ is desirably close to zero and (ii) robust estimations. Moreover, the PDF mass very close to the $c = 0$ axis (shape index is undefined for a plane) is also negligible: $P_{\mathcal{M}}(c < c_{\min}, s \in [-1, 1]) < \delta$ for sufficiently small $c_{\min}, \delta$. This paper sets $c_{\min} = 0.001$.

4 New Approach to Multivariate Histogram Testing

Having estimated the folding pattern descriptors for a group of N surfaces in a clinical study, namely $P_{\mathcal{M}^1}(C, S), \ldots, P_{\mathcal{M}^N}(C, S)$, this section proposes a novel application of a known nonparametric permutation-based approach for statistical hypothesis testing for multivariate histograms.

Typical hypothesis tests (cross-sectional, longitudinal, regression) are subsumed in the framework of general linear models (GLM). The GLM framework has been applied extensively for *voxel-based* neuroimaging studies of brain function and structure, which entail running parametric GLM tests at each voxel in the image followed by corrections for multiple comparisons via, for instance, random field theory. However, this parametric approach makes strong assumptions

on the data concerning the parametric distributions of the values at each point in the domain and the dependencies between the neighborhoods. Such strategies can be prone to spurious results when these assumptions become invalid. Permutation tests, on the other hand, are nonparametric and rely on the *less inclusive* assumption that the observations are *exchangeable*, thereby making the tests more stringent. Under the permutation-test null hypothesis, i.e. both groups of surfaces being generated by one distribution, the independent and identically-distributed observations are exchangeable. A rigorous hypothesis testing scheme based on nonparametric permutation testing for *voxel-based* studies is statistical nonparametric mapping (SnPM) [25].

We propose a novel application of SnPM for multivariate high-dimensional histogram analysis. This scheme differs from (i) conventional use of SnPM for studies in the image domain [25] or surface domain [27] domain, and (ii) typical parametric tests (e.g. Hotelling T^2) for histogram analysis which fail to inform the location, in the histogram domain, for a significant difference/effect. The algorithm is as follows:

1. Empirically select thresholds $c_{\min} > 0$ and $c_{\max}$ for curvedness values and a very small ϵ such that, $\forall n = 1, \ldots, N$; $P_{\mathcal{M}^n}(c \notin [c_{\min}, c_{\max}], s \notin [-1, 1]) < \epsilon$.
2. For the domain $[c_{\min}, c_{\max}] \times [-1, 1]$, construct a regular rectangular tessellation of the desired resolution. Denote the resulting IJ rectangular bins by $\{b_{ij} :: i = 1, \ldots, I; j = 1, \ldots, J\}$. This paper sets $I = J = 64$; finer resolutions increase computation time.
3. For all surfaces $n = 1, \ldots, N$ and all bins $\{b_{ij}\}$, compute the probabilities $P_{\mathcal{M}^n}((c, s) \in b_{ij})$ denoted in short by $P_n(i, j)$. Note that $0 \leq P_n(i, j) \leq 1$ justifying a nonparametric testing approach for accuracy and reliability.
4. Use the N 2D images of probability values, $P_1, \ldots, P_N$, as input for SnPM [25]. SnPM will produce (i) a set of *locations* ij and (ii) a set of *clusters* exhibiting statistical significance for the underlying GLM experiment. Figure 2 shows an example study which is explained in detail later in Section 5.2.

5 Validation and Results

5.1 Cortical Folding Pattern Analysis Pipeline

The clinical study in this paper employed the following processing sequence: (i) brain extraction, ROI parcellation [28], denoising, inhomogeneity correction, and contrast enhancement via adaptive histogram equalization (ii) automatic intensity-based probabilistic tissue segmentation [29]; (iii) resample the segmentation to an isotropic voxel size of 0.4 mm^3; (iv) define $\mathcal{M}$ to be the cortical gray-white interface corresponding to a cortical-white-matter membership of 0.5 (gray-white interface estimated much more reliably than gray-fluid interface, especially in neonatal/pediatric populations); (v) represent cortical surface $\mathcal{M}$ in the ROI, to subvoxel accuracy, as a level set [24] (vi) compute curvedness $C(m)$ and shape-index $S(m)$ values at every voxel m on the level set $\mathcal{M}$, (vii) estimate the proposed multivariate folding pattern descriptor $P_{\mathcal{M}}(C, S)$ in the operculum as described in

Section 3, (viii) perform multivariate statistical hypothesis testing as described in Section 4. The implementation and visualization in this paper relied on the Insight Toolkit (ITK), Matlab, ITK-SNAP, and the Visualization Toolkit (VTK).

5.2 Validation via Clinical and Simulated Adult Data

Cortical Shape Asymmetry in Normal Adults: The first validation experiment used 50 MR images of normal adults and measured the average fraction of cortical surface area embedded in sulci. The left halves, i.e. $S < 0$, of the plots concern concave patches (associated with sulci), while the right halves, i.e. $S > 0$, concerns convex patches (associated with gyri). The mass in the left half of the mean PDF of all images, i.e. $P_{\text{mean}}(S < 0; C \geq 0)$ is a robust estimate of the fraction of the surface area of the cortical surface buried in sulci. We estimated this fraction to be 0.58 for the frontal, parietal, and temporal lobes in adults, which comes very close to the published value of 0.61 for gray-white interfaces of entire brains [18,15]. For the occipital lobes, however, our estimate of this fraction was lower, equal to 0.54. Figure 3 shows this phenomenon clearly, i.e. the PDF in Figure 3(d) has more mass (red) on the right (convex gyral regions) relative to the PDFs in Figure 3(a)-(c). These experiments demonstrate that the proposed descriptor is sensitive to changes in cortical *shape*.

Simulated Complexity Differences using BrainWeb Data: We validated the proposed framework for folding pattern analysis using 20 simulated images from the BrainWeb [26] repository having ground-truth segmentations. We conducted a cross sectional study between (i) the group of gray-white surfaces in the BrainWeb images and (ii) another group of surfaces obtained after slightly smoothing the surfaces in the first group (mean curvature flow, time step 0.24, iterations 4). Figure 1(d)-(g) show values of C and S painted on a cortical surface and its smoothed version. Figure 2(a) and (b) show the means of the surface descriptors $P_{\mathcal{M}^n}(C, S)$ in the two groups. As expected, the smoothed surfaces have a mean PDF (Figure 2(b)) shifted slightly downwards, i.e. regions of low curvature, relative to Figure 2(a). The t-statistic map (Figure 2(c)) clearly reveals the

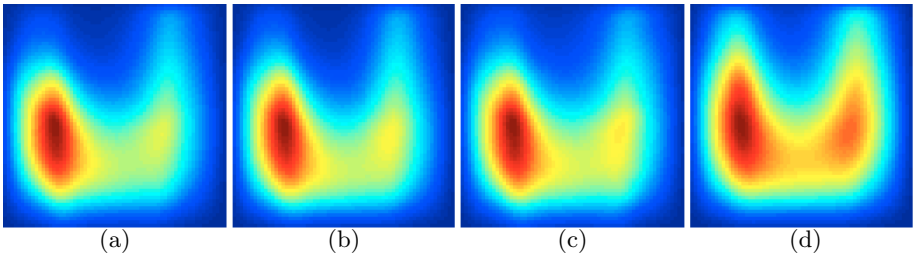

Fig. 3. Validation : measuring the fraction of surface area of the cortical gray-white surface embedded in sulci (concave surface patches) in 50 normal adults. **(a)-(d)** Proposed surface descriptors for the frontal, parietal, temporal, and occipital lobes, respectively.

difference between the two groups. The blue (or red) significant locations (Figure 2(d)), at level of significance $\alpha = 0.05$, correspond to those locations whose t statistics were less than (or greater than) the lowest (or greatest) 100α-th percentile of the permutation distribution of the smallest (or largest) t statistic over the $< C, S >$ domain. Similarly, significant clusters (in all figures in this paper) are shown in blue (or red) when the sizes of the clusters formed by thresholding the negative (or positive) t statistics are larger than the 100α-th percentile of the permutation distribution of the maximum cluster size obtained after thresholding the negative (or positive) t statistics. Figure 2(d) shows that the proposed framework correctly indicates that the differences between the groups are in cortical complexity alone, *not* in cortical shape.

5.3 Neonatal CHD Cohort, Imaging, and Image Analysis

The clinical cohort comprised 42 neonates with complex CHD (29 with HLHS, 13 with TGA) between 1−2 weeks of age, *before* undergoing corrective heart surgery. MR images were acquired on a 3T scanner (Siemens Trio) with voxel sizes around 0.88x0.88x1.5 mm^3 using T1-weighted, T2-weighted, and FLAIR schemes. The HLHS and TGA groups were well matched by age *and brain volume*. The left and right opercula in every image were parcellated semi-automatically with expert supervision. Brain tissue segmentation was performed via [29].

5.4 Folding Differences between Normal and Abnormal Opercula

Before studying opercular differences in HLHS and TGA, we first study the differences between normal and abnormal opercular folding complexity and shape. Figure 4 shows the differences in the surface descriptors of two neonates selected by a pediatric neurologist from the clinical cohort, one with the closest-to-normal operculum (mature, "closed", folded) and another with the farthest-from-normal

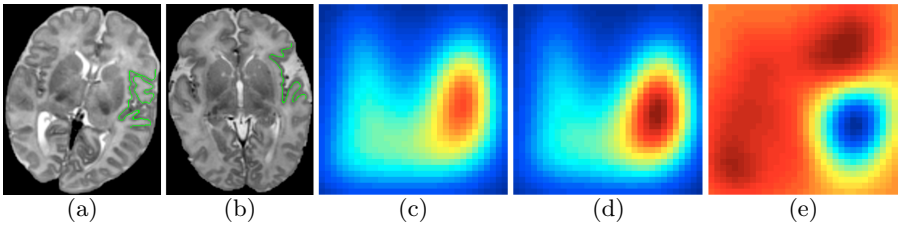

Fig. 4. **(a)-(b)** Example MR images of the normal (mature, "closed", more folded) and farthest-from-normal (immature, "open", less folded) opercula, respectively, overlapped with the extracted cortical surfaces. **(c)-(d)** Average cortical folding descriptors $P_{\text{average normal}}(C, S)$ and $P_{\text{average abnormal}}(C, S)$ for 2 closest-to-normal and 4 significantly-abnormal opercula, respectively, chosen by a medical expert based on a subjective clinical scoring protocol [9]. **(e)** $P_{\text{average normal}}(C, S) - P_{\text{average abnormal}}(C, S)$; blue ≡ negative and red ≡ positive values.

operculum (immature, "open", less folded). Figure 4(e) indicates that normal opercula have (i) a larger fraction of surface patches that have higher curvature (implying more complex folding) and (ii) a larger fraction of surface patches that are concave (implying more "closed" shape). We compared these findings to qualitative studies of immature opercula in neonates [6,7] that provide drawings of immature opercular cortical surfaces. The analysis in this paper shows that, relative to normal opercula, abnormal opercula in CHD may exhibit lesser folding complexity and may be more "open". This also indicates that brain maturation concerns *not* only cortical complexity, but cortical shape as well.

5.5 Folding Differences between HLHS and TGA Opercula

Figure 5 shows the differences in folding complexity and shape between HLHS and TGA. Establishing analogies between Figure 5 and Figure 4, we find that while TGA neonates have a larger fraction of high-curvature patches, HLHS neonates have a large fraction of concave low-curvature surface patches. Since it is known via subjective clinical-scoring-based studies that the opercula are immature in both HLHS and TGA [9], the analysis in this paper suggests that HLHS and TGA might affect opercular development in different ways, i.e. while HLHS might cause greater reductions in opercular folding complexity, TGA might cause more "open" opercula. A cross-sectional study between CHD neonates and normal neonates would be very interesting and probably yield much more significant differences, but such data has been elusive so far. Nevertheless, this is an important aspect of future work.

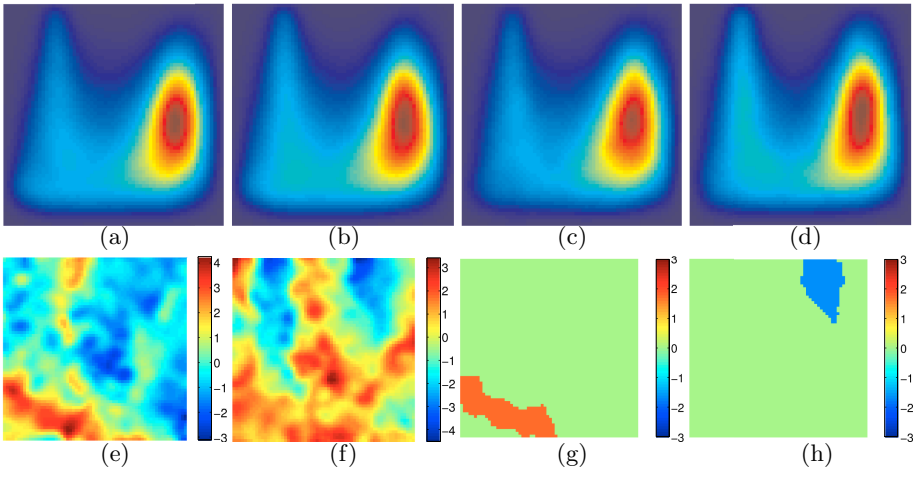

Fig. 5. **(a)-(b)** Average of cortical folding descriptors $P(C, S)$ in right and left opercula, respectively, for 29 neonates with HLHS. **(c)-(d)** Average of the descriptors in right and left opercula, respectively, for 12 neonates with TGA. **(e)-(f)** t-statistic maps; $t > 0 \Rightarrow P_{\text{HLHS}} > P_{\text{TGA}}$. for right and left opercula, respectively. **(g)-(h)** Significant clusters found via SnPM [25] for right and left opercula, respectively.

6 Conclusion

The paper proposes a novel multivariate statistical descriptor of folding patterns in a high-dimensional space. PDF-based shape descriptors in the literature that come closest to the proposed method analyze histograms of either shape-indices or curvatures (*not* both) and produce low-dimensional descriptors: [5] and [20] propose 2-valued and 9-valued descriptors, respectively. On the other hand, the proposed descriptor is a continuous function informing about both surface shape and complexity. Unlike [20] which shows concern about the dimensionality of their descriptor, the proposed framework effectively deals with dimensionality by a novel application of a rigorous hypothesis-testing framework. The experiments establish a link between the proposed descriptor and published qualitative studies of normal/abnormal opercular folding [6,7] to demonstrate how the proposed descriptor can be interpreted for opercular studies. The proposed framework can be easily extended to (i) include other cortical information, e.g. thickness, and (ii) study other specific anatomical structures or ROIs. The rigorous theoretical underpinning coupled with the ease of implementation can facilitate sophisticated studies of surfaces with relatively less effort.

References

1. Thompson, P., Lee, A., Dutton, R., Geaga, J., Hayashi, K., Eckert, M., Bellugi, U., Galaburda, A., Korenberg, J., Mills, D., Toga, A., Reiss, A.: Abnormal cortical complexity and thickness profiles mapped in Williams syndrome. J. Neuroscience 25(16), 4146–4158 (2005)
2. Nordahl, C., Dierker, D., Mostafavi, I., Schumann, C., Rivera, S., Amaral, D., Van-Essen, D.: Cortical folding abnormalities in autism revealed by surface-based morphometry. Journal of Neuroscience 27(43), 11725–11735 (2007)
3. Batchelor, P., Castellano-Smith, A., Hill, D., Hawkes, D., Cox, T., Dean, A.: Measures of folding applied to the development of the human fetal brain. IEEE Trans. Med. Imaging 21(8), 953–965 (2002)
4. Yu, P., Grant, P.E., Qi, Y., Han, X., Segonne, F., Pienaar, R., Busa, E., Pacheco, J., Makris, N., Buckner, R.L., Golland, P., Fischl, B.: Cortical surface shape analysis based on spherical wavelets. IEEE Trans. Med. Imaging 26(4), 582–597 (2007)
5. Pienaar, R., Fischl, B., Caviness, V., Makris, N., Grant, P.E.: A methodology for analyzing curvature in the developing brain from preterm to adult. Int. J. Imaging Systems Technology 18(1), 42–68 (2008)
6. Chen, C., Zimmerman, R., Faro, S., Parrish, B., Wang, Z., Bilaniuk, L., Chou, T.: MR of the cerebral operculum: abnormal opercular formation in infants and children. American Journal of Neuroradiology 17(7), 1303–1311 (1996)
7. Childs, A., Ramenghi, L., Cornette, L., Tanner, S., Arthur, R., Martinez, D., Levene, M.: Cerebral maturation in premature infants: Quantitative assessment using MR imaging. Amer. J. of Neuroradiology 22, 1577–1582 (2001)
8. Miller, S., McQuillen, P., Hamrick, S., Xu, D., Glidden, D., Charlton, N., Karl, T., Azakie, A., Ferriero, D., Barkovich, J., Vigneron, D.: Abnormal brain development in newborns with congenital heart disease. New Eng. J. Med. 357, 1928–1938 (2007)
9. Licht, D., Shera, D., Clancy, R., Wernovsky, G., Montenegro, L., Nicolson, S., Zimmerman, R., Spray, T., Gaynor, W., Vossough, A.: Brain maturation is delayed in infants with complex congenital heart defects. J. Thorac. Cardiovasc. Surg. 137, 529–537 (2009)

10. Tosun, D., Duchesne, S., Rolland, Y., Toga, A., Verin, M., Barillot, C.: 3D analysis of cortical morphometry in differential diagnosis of Parkinson's Plus Syndromes. In: Ayache, N., Ourselin, S., Maeder, A. (eds.) MICCAI 2007, Part II. LNCS, vol. 4792, pp. 891–899. Springer, Heidelberg (2007)
11. Van-Essen, D., Dierker, D.: Surface-based and probabilistic atlases of primate cerebral cortex. Neuron 56, 209–225 (2007)
12. Mangin, J., Riviere, D., Cachia, A., Duchesnay, E., Cointepas, Y., Papadopoulos-Orfanos, D., Scifo, P., Ochiai, T., Brunelle, F., Regis, J.: A framework to study the cortical folding patterns. NeuroImage 23(1), S129–S138 (2004)
13. Lyttelton, O., Boucher, M., Robbins, S., Evans, A.: An unbiased iterative group registration template for cortical surface analysis. NeuroImage 34, 1535–1544 (2007)
14. Thompson, P., Schwartz, C., Lin, R., Khan, A., Toga, A.: Three-dimensional statistical analysis of sulcal variability in the human brain. J. Neurosci. 16(13), 4261–4274 (1996)
15. Van-Essen, D., Drury, H.: Structural and functional analyses of human cerebral cortex using a surface-based atlas. J. Neuroscience 17(18), 7079–7102 (1997)
16. Awate, S.P., Win, L., Yushkevich, P., Schultz, R.T., Gee, J.C.: 3D cerebral cortical morphometry in autism: Increased folding in children and adolescents in frontal, parietal, and temporal lobes. In: Proc. Int. Conf. Med. Image Comput. Comp. Assist. Interv., vol. 1, pp. 559–567 (2008)
17. Griffin, L.: The intrinsic geometry of the cerebral cortex. J. Theor. Biol. 166(3), 261–273 (1994)
18. Zilles, K., Armstrong, E., Schleicher, A., Kretschmann, H.: The human pattern of gyrification in the cerebral cortex. Anat. Embryol. 179, 173–179 (1988)
19. Koenderink, J., van Doorn, A.: Surface shape and curvature scales. Image and Vision Computing 10(8), 557–565 (1992)
20. Akgul, C., Sankur, B., Schmitt, F., Yemez, Y.: Multivariate density-based 3D shape descriptors. In: Int. Conf. Shape Modeling and Appl., pp. 3–12 (2007)
21. Papoulis, A., Pillai, S.U.: Probability, Random Variables, and Stochastic Processes, 4th edn. McGraw-Hill, New York (2001)
22. Lu, Z., Chen, X.: Spatial kernel regression estimation: weak consistency. Stat. and Prob. Letters 68(2), 125–136 (2004)
23. Chow, Y., Geman, S., Wu, L.: Consistant cross-validated density estimation. Annals of Statistics 11(1), 25–38 (1983)
24. Osher, S., Paragios, N.: Geometric Level Set Methods in Imaging, Vision, and Graphics. Springer, Heidelberg (2003)
25. Nichols, T., Holmes, A.: Nonparametric permutation tests for functional neuroimaging: a primer with examples. Human Brain Mapping 15(1), 1–25 (2002)
26. Aubert-Broche, B., Collins, D., Evans, A.: Twenty new digital brain phantoms for creation of validation image data bases. IEEE Trans. Med. Imag. 25(11), 1410–1416 (2006)
27. Styner, M., Gerig, G.: Correction scheme for multiple correlated statistical tests in local shape analysis. In: SPIE Medical Imaging, pp. 233–240 (2003)
28. Avants, B., Gee, J.: Geodesic estimation for large deformation anatomical shape averaging and interpolation. Neuroimage 23(1), 139–150 (2004)
29. Song, Z., Awate, S.P., Licht, D., Gee, J.: Clinical neonatal brain MRI segmentation using adaptive nonparametric data models and intensity-based Markov priors. In: Proc. Med. Image Comput. Comp. Assist. Interv., vol. 1, pp. 883–890 (2007)